Revision 1

Rongibbsite, $Pb_2(Si_4Al)O_{11}(OH)$, a new zeolitic aluminosilicate mineral with an interrupted framework from Maricopa County, Arizona, USA

Hexiong Yang, Robert T. Downs, Stanley H. Evans, Robert A. Jenkins, and Elias M. Bloch
Department of Geosciences, University of Arizona, 1040 E. 4th Street, Tucson, AZ 85721-0077, U.S.A.

Abstract

A new zeolitic aluminosilicate mineral species, rongibbsite, ideally $Pb_2(Si_4Al)O_{11}(OH)$, has been found in a quartz vein in the Proterozoic gneiss of the Big Horn Mountains, Maricopa County, Arizona, U.S.A. The mineral is of secondary origin and is associated with wickenburgite, fornacite, mimetite, murdochite, and creaseyite. Rongibbsite crystals are bladed (elongated along the *c* axis, up to 0.70 × 0.20 × 0.05 mm), often in tufts. Dominant forms are {100}, {010}, {001} and {10 -1}. Twinning is common across (100). The mineral is colorless, transparent with white streak and vitreous luster. It is brittle and has a Mohs hardness of ~5; cleavage is perfect on {100} and no parting was observed. The calculated density is 4.43 g/cm^3. Optically, rongibbsite is biaxial (+), with $n_\alpha = 1.690$, $n_\beta = 1.694$, $n_\gamma = 1.700$, c^Z = 26 º, $2V_{meas} = 65(2)$º. It is insoluble in water, acetone, or hydrochloric acid. Electron microprobe analysis yielded an empirical formula $Pb_{2.05}(Si_{3.89}Al_{1.11})O_{11}(OH)$.

Rongibbsite is monoclinic, with space group *I*2/*m* and unit-cell parameters a = 7.8356(6), b = 13.913(1), c = 10.278(1) Å, β = 92.925(4)°, and V = 1119.0(2) Å^3. Its structure features an interrupted framework made of three symmetrically-distinct TO_4 tetrahedra (T = Si + Al). The framework density is 17.9 T per 1000 Å^3. Unlike many known interrupted frameworks in zeolite-type materials, which are usually broken up by OH or F, the framework in rongibbsite is interrupted by O atoms. There are a variety of corner-shared tetrahedral rings in the framework of rongibbsite, including two types of 4-membered, three 6-membered, and one 8-membered rings. The extraframework Pb and OH reside alternately in the channels formed by the 8-membered rings. The Pb cations are disordered over two split sites, Pb and Pb', with site-occupancies of 0.8 and 0.2, respectively, and a Pb—Pb' distance of 0.229 Å, providing a structural explanation for the two strong Raman bands (at 3527 and 3444 cm^{-1}) attributable to the O-H stretching vibrations. The average bond lengths for the T1, T2, and T3 tetrahedra are 1.620, 1.648, and 1.681 Å, respectively, indicating that the preference of Al for the three tetrahedral sites is T3 >> T2 > T1. Rongibbsite represents the first natural aluminosilicate with Pb as the only extraframework cation.

***Key words*:** rongibbsite, zeolitic aluminosilicate, Pb-bearing, interrupted framework, crystal structure, X-ray diffraction, Raman spectra

Introduction

A new zeolitic aluminosilicate mineral species, rongibbsite, ideally $Pb_2(Si_4Al)O_{11}(OH)$, has been found in the Big Horn Mountains, Maricopa County, Arizona, U.S.A. It is named after its finder, Mr. Ronald Bradford Gibbs, a mineral collector and a mining geologist in Tucson, Arizona. The new mineral and its name have been approved by the Commission on New Minerals, Nomenclature and Classification (CNMNC) of the International Mineralogical Association (IMA2010-055). Part of the cotype sample has been deposited at the University of Arizona Mineral Museum (Catalogue # 19292) and the RRUFF Project (deposition # R100031). In this paper, we describe the physical and chemical properties of rongibbsite and its structural features determined from single-crystal X-ray diffraction and Raman spectroscopy. Along with the zeolite maricopaite, $Ca_2Pb_7(Si_{36}Al_{12})O_{99}\cdot n(H_2O,OH)$, found in the same region (Rouse and Peacor 1994), rongibbsite joins a small group of natural and synthetic compounds that possess interrupted tetrahedral framework structures. While maricopaite is the only natural zeolite having Pb as a dominant extraframework cation, rongibbsite represents the first natural aluminosilicate with Pb as the only extraframework cation.

Sample Description and Experimental Methods

Occurrence, physical and chemical properties, and Raman spectra

Rongibbsite was found in material collected from a small unnamed prospect in the Big Horn District, Big Horn Mountains, Maricopa County, Arizona, U.S.A (lat. 33°69' N and long. 113°22'). Rongibbsite occurs with other secondary lead and copper minerals in a quartz vein in Proterozoic gneiss. Mineral occurrences in the Big Horn district are gold-rich, basement hosted narrow quartz pods and veins associated with late Cretaceous intrusives (Allen, 1985). Associated minerals are wickenburgite, fornacite, mimetite, murdochite, and creaseyite. Other minerals found in the quartz veins include: anglesite, cerussite, chrysocolla, iranite, gold, mottramite, willemite, phoenicochroite, planchéite, iron oxides, the sulfides galena and chalcopyrite, and zeolites including stilbite, heulandite, and laumontite. Rongibbsite crystals are bladed (elongated along the *c* axis) (up to 0.70 × 0.20 × 0.05 mm), often in tufts (Fig. 1). Dominant forms are {100}, {010}, {001} and {10 -1}. Twinning is common on (100). The mineral is colorless, transparent with white streak and vitreous luster. It is brittle and has a Mohs hardness of ~5; cleavage is perfect on {100} and no parting was observed. The calculated density is 4.43 g/cm^3 using the empirical formula. Optically, rongibbsite is biaxial (+), with $n_\alpha = 1.690$, n_β =1.694, $n_\gamma = 1.700$, c^Z = 26 º, $2V_{meas} = 65(2)$º, and $2V_{calc} = 66$ º. The dispersion is strong ($r > v$). The compatibility index ($1-K_p/K_c$) is 0.019 (superior). It is insoluble in water, acetone, or hydrochloric acid.

The chemical composition was determined with a CAMECA SX50 electron microprobe at 15 kV and 5 nA with a beam diameter of 20 μm (http://rruff.info/rongibbsite). The standards used include diopside for Si, anorthite for Al, and Pb-glass (NIST-K0229) for Pb, yielding an average composition (wt.%) (11 points) of SiO_2 30.64(15), Al_2O_3 7.44(19), PbO 59.80(40), $H2O^+$ 1.18 (estimated for charge balance), and total = 99.06(47). The resultant chemical formula, calculated on the basis of 12 O atoms (from the structure determination), is $Pb_{2.05}(Si_{3.89}Al_{1.11})O_{11}(OH)$, which can be simplified as $Pb_2(Si_4Al)O_{11}(OH)$.

The Raman spectrum of rongibbsite was collected on a randomly oriented crystal from 15 scans at 30 s and 100% power per scan on a Thermo Almega microRaman system, using a solid-state laser with a frequency of 532 nm and a thermoelectric cooled CCD detector. The laser is partially polarized with 4 cm^{-1} resolution and a spot size of 1 μm.

X-ray crystallography

Because of the limited amount of available material, no powder X-ray diffraction data were measured for rongibbsite. Listed in Table 1 are the powder X-ray diffraction data calculated from the determined structure using the program XPOW (Downs et al. 1993). Single-crystal X-ray diffraction data were collected from a nearly equi-dimensional, untwinned crystal (0.03 × 0.04 x 0.05 mm) on a Bruker X8 APEX2 CCD X-ray diffractometer equipped with graphite-monochromatized MoKα radiation with frame widths of 0.5° in ω and 30 s counting time per frame. All reflections were indexed on the basis of a monoclinic unit-cell (Table 2). The intensity data were corrected for X-ray absorption using the Bruker program SADABS. The systematic absences of reflections suggest possible space group *C*2, *Cm*, or *C2/m*. The crystal structure was solved and refined using SHELX97 (Sheldrick 2008) based on the space group *C2/m*, because it yielded the best refinement statistics in terms of bond lengths and angles, atomic displacement parameters, and *R* factors. However, to avoid the large β angle (125.463º) in the *C*-lattice setting, we adopted space group *I*2/*m* (β = 92.925º) in this study. A preliminary structure refinement based on the ideal chemical formula revealed an outstanding residual peak in the proximity of the Pb site on the difference Fourier maps. A site-split model for Pb was, therefore, introduced in the subsequent refinements, with the occupancies of Pb at the two sites allowed to vary. No site occupancies were refined between Si and Al among the three tetrahedral sites (T1, T2, and T3), due to their similar X-ray scattering power. For simplicity, all Al atoms were assigned to the T3 site during the refinement because the average bond distance for this site (1.681 Å) is significantly longer than that for the T1 (1.620 Å) or T2 site (1.648 Å), both of which were assumed to be filled with Si during the refinement. The positions of all atoms were refined with anisotropic displacement parameters, except for the H atom, which was refined with a fixed isotropic displacement parameter (U_{iso} = 0.03). Final coordinates and displacement parameters of atoms in rongibbsite are listed in Table 3, and selected bond-distances in Table 4.

Discussion

Crystal Structure

The crystal structure of rongibbsite is characterized by an interrupted framework consisting of three crystallographically-distinct TO_4 tetrahedra (T = Si + Al), with the bonded extraframework Pb and OH residing alternately in channels extending along the *b*-axis (Fig. 2). The framework density is 17.9 T per 1000 Å^3, which falls right in the region for zeolite-type frameworks (Brunner and Meier 1989). However, unlike many known interrupted frameworks in zeolite-type materials, which are usually broken up by OH or F (Smith 1988; Coombs et al. 1998), the framework in rongibbsite is interrupted by an O atom (O1). Interestingly, the Pb-bearing zeolite mineral maricopaite, which was found in the same region (Maricopa County, Arizona) as rongibbsite, also exhibits a tetrahedral framework interrupted by O atoms (Rouse and Peacor 1994).

The framework of rongibbsite can also be visualized as built of tetrahedral sheets (Fig. 3) linked together along (101) by sharing the vertex O atoms between $T2O_4$ tetrahedra. There are several kinds of symmetrically-distinct tetrahedral rings in the framework, including one 8-membered, three 6-membered, and two 4-membered rings (Fig. 4). The intricate arrangements of these rings are illustrated in Figure 5. The extraframework Pb cations are situated in the channels formed by 8-membered rings and distributed over two split sites, Pb and Pb', with site-occupancies of 0.8 and 0.2, respectively, and a Pb—Pb' distance of 0.229 Å. Site-splitting for Pb is quite common, especially in materials constructed of framework structures (e.g., Szymanski 1988; Moore et al. 1989, 1991; Gunter et al. 1994; Holtstam et al. 1995; Downs et al. 1995; Tribaudino et al. 1998; Siidra et al. 2009). It is worth noting that the Si/Al ratio in the structure is also about 0.8/0.2, the same as the Pb occupancies between the two split sites. Perhaps the Pb site-splitting is a requirement of the $(Si_4Al)O_{11}$ network configuration. The average bond lengths for the T1, T2, and T3 tetrahedra are 1.620, 1.648, and 1.681 Å, respectively, indicating the predominant ordering of Al in the T3 site and the possible substitution of some Al for Si at the T2 site. The T3 tetrahedron is also the most distorted of the three TO_4 groups, as measured by the tetrahedral angle variance (TAV) and quadratic elongation (TQE) (Robinson et al. 1971), which are 4.62 and 1.001 for T1, respectively, 2.53 and 1.001 for T2, and 21.76 and 1.006 for T3.

A calculation of bond-valence sums for rongibbsite (Table 5) using the parameters given by Brese and O'Keeffe (1991) shows that O6 is relatively underbonded, suggesting that it may be engaged in the hydrogen bonding, although the O6…H distance (2.98 Å) seems to be a little too long for a meaningful hydrogen bond. The tetrahedral site occupancies estimated from the bond-valence sums yield T1 = Si, T2 = 0.8 Si + 0.2 Al, and T3 = 0.4 Si + 0.6 Al. As the Pb-Pb' splitting vector points directly towards the T2 site, with Pb' 0.212 Å closer to T2 than Pb, it is possible that the 20% Al occupancy at the T2 site provides the electrostatic mechanism that splits Pb'.

Raman spectra

Raman spectroscopy has been extensively employed to gain comprehensive structural information of various zeolite-type and feldspar-type aluminosilicate materials (e.g., Dutta et al. 1988, 1992; Smirnov et al. 1994; Wopenka et al. 1998; Goryainov and Smirnov 2001; Yu et al. 2001; Mozgawa et al. 2004; Putnis et al. 2007; Fisch et al. 2008; Liu et al. 2012). Presented in Figure 5 is the Raman spectrum of rongibbsite. Based on previous studies on aluminosilicate materials with the framework structures, we made a tentative assignment of major Raman bands for rongibbsite. The two strong bands at 3527 and 3444 cm^{-1} are ascribed to the O-H stretching vibrations. The bands between 900 and 1100 cm^{-1} and those between 600 and 700 cm^{-1} are attributable to the T-O anti-symmetric and symmetric stretching vibrations (ν_3 and ν_1 modes) within the TO_4 groups, respectively. Major bands in the region ranging from 250 to 550 cm^{-1} originate from the T-O-T bending vibrations. The bands below 250 cm^{-1} are mostly associated with the rotational and translational modes of TO_4 tetrahedra, as well as the lattice vibrational modes. Remarkably, there is only one OH site in the rongibbsite structure, but its Raman spectrum displays two distinct peaks in the O-H stretching region. This observation is likely a direct consequence of the disordering of Pb over the two split sites, as O8H is bonded solely to Pb in the structure, which also accounts for the largest isotropic displacement parameter for O8H among all O atoms (Table 3). Integration of the two OH peaks indicate that 25% of the OH peak intensity is in the 3527 cm^{-1} peak while 75% is in the 3444 cm^{-1} peak, consistent with the Pb-site occupancies. The nature of the weak and broad band at ~2900 cm^{-1} is unclear. Similar weak and broad bands have also been observed in other hydrous minerals from IR and Raman spectra, such as lawsonite (e.g., Libowitzky and Rossman 1996; Kolesov et al. 2008) and zeolites (e.g., Wopenka et al. 1998; Gujar et al. 2005). In lawsonite, this band has been assigned to the O-H stretching vibrations due to a strong hydrogen bond with an O-H···O distance of ~2.60 Å and an

H···O distance of 1.60-1.65 Å (Libowitzky and Rossman 1996; Kolesov et al. 2008). However, there is no O atom within 3.0 Å around O8H in rongibbsite.

As in other zeolite-type and tectosilicate compounds, including quartz and feldspars, the Raman bands assigned to the T-O symmetric stretching vibrations in rongibbsite are noticeably weaker than those ascribable to the T-O asymmetric stretching modes, resulting primarily from the complex vibrations of TO_4 tetrahedra coupled through sharing of their vertex O atoms (Wopenka et al. 1998). In contrast, for materials containing isolated TO_4 tetrahedra, the Raman bands caused by T-O symmetric stretching modes are typically much stronger than the ones arising from T-O asymmetric stretching modes.

It has been well established that the wavenumbers of Raman bands attributable to the T-O-T bending modes are inversely correlated to the tetrahedral ring size or the average <T-O-T> angle for a given tetrahedral ring, as well as the Si/Al ratio (e.g., Dutta et al. 1992; Wopenka et al. 1998; Yu et al. 2001). In particular, based on the UV Raman spectroscopic measurements, Yu et al. (2001) demonstrated that the Raman bands at 470-530, 370-430, 290-410, and 220-280 cm^{-1} can be assigned to the bending modes of 4-, 5-, 6-, and 8-membered rings of aluminosilicate zeolites, respectively. This explains the complex Raman pattern between 250 and 550 cm^{-1} for rongibbsite, as it contains a mixture of 4-, 6-, and 8-membered tetrahedral rings in its framework structure.

Acknowledgements

This study was funded by the Science Foundation Arizona.

References Cited

Allen, G.B. (1985) Economic Geology of the Big Horn Mountains of West-Central Arizona. Arizona Geological Survey, Open File Report, 85-17.

Gujar, A.C., Moye, A.A., Coghill, P.A., Teeters, D.C., Roberts, K.P., Price, G.L. (2005) Raman investigation of the SUZ-4 zeolite. Microporous and Mesoporous Materials, 78, 131-137.

Brese, N.E. and O'Keeffe, M. (1991) Bond-valence parameters for solids. Acta Crystallographica, B47, 192-197.

Brunner, G.O. and Weier, W.M. (1989) Framework density distribution of zeolite-type tetrahedral nets. Nature, 337, 146.

Coombs, D.S., Alberti, A., Armbruster, T., Artioli, G., Galli, E., Grice, J.D., Liebau, F., Mandarino, J.A., Nickel, E.H., Passaglia, E., Peacor, D.R., Quartieri, S., Rinaldi, R., Ross, M., Sheppard, R.A., Tillmanns, E., and Vezzalini, G. (1998) Recommended nomenclature for zeolite minerals: report of the subcommittee on zeolites of the International Mineralogical Association, Commission on New Minerals and Mineral Names. Mineralogical Magazine, 62, 533-571.

Downs, R.T., Bartelmehs, K.L., Gibbs, G.V. and Boisen, M.B., Jr. (1993) Interactive software for calculating and displaying X-ray or neutron powder diffractometer patterns of crystalline materials. American Mineralogist, 78, 1104-1107.

Downs, R.T., Hazen, R.M., Finger, L.W. and Gasparik, T. (1995) Crystal chemistry of lead aluminosilicate hollandite: A new high-pressure synthetic phase with octahedral silicon. American Mineralogist, 80, 937-940.

Dutta, P.K., Shieha, D.C., and Puria, M. (1988) Correlation of framework Raman bands of zeolites with structure. Zeolites, 8, 306–309.

Dutta, P.K., Rao, K.M., and Park, J.Y. (1992) Vibrational spectroscopic study of the evolution of the framework of the zeolite ferrierite. Langmuir, 8, 722-726.

Fisch, M., Armbruster, T., and Kolesov, B. (2008) Temperature-dependent structural study of microporous CsAlSi5O12. Journal of Solid State Chemistry, 181, 423-431.

Goryainov, S.V. and Smirnov, M.B. (2001) Raman spectra and lattice-dynamical calculations of natrolite. European Journal of Mineralogy, 13, 507–519.

Gunter, M.E., Armbruster, T., Kohls, T., and Knowles, C.R. (1994) Crystal structure and optical properties of Na- and Pb-exchanged heulandite-group zeolites. American Mineralogist, 79, 675-682.

Holtstam, D., Norrestam, R., Sjödin, A. (1995) Plumboferrite: new mineralogical data and atomic arrangement, American Mineralogist 80, 1065-1072.

Kolesov, B.A., Lager, G.A., and Schultz, A.J. (2008) Behaviour of H2O and OH in lawsonite: a single-crystal neutron diffraction and Raman spectroscopic investigation. European Journal of Mineralogy, 20, 63-72.

Libowitzky, E. and Rossman, G.R. (1996) FTIR spectroscopy of lawsonite between 82 and 325 K. American Mineralogist, 81, 1080-1091.

Liu, D., Liu, Z., Lee, Y., Seoung, D., and Lee, Y. (2012) Spectroscopic characterization of alkali-metal exchanged natrolites. American Mineralogist, 97, 419-424.

Moore, P.B, Gupta, P.K.S., Page, Y.L. (1989) Magnetoplumbite, $Pb^{2+}Fe^{3+}{}_{12}O_{19}$: refinement and lone-pair splitting. American Mineralogist, 74, 1186-1194.

Moore, P.B., Sen Gupta, R.K., Shen, J., Schlemper, E.O. (1991) The kentrolite-melanotekite series, $4Pb_2(Mn,Fe)^{3+}{}_2O_2[Si_2O_7]$: Chemical crystallographic relations, lone-pair splitting, and cation relation to $8URe_2$. American Mineralogist, 76, 1389-1399.

Mozgawa, W., Handke, M., and Jastrzebski, W. (2004) Vibrational spectra of aluminosilicate structure clusters. Journal of Molecular Structure, 704, 247-257.

Putnis, C.V., Geisler, T., Schmid-Beurmann, P., Stephan, T., and Giampaolo, C. (2007) An experimental study of the replacement of leucite by analcime. American Mineralogist, 92, 19-26.

Robinson, K., Gibbs, G.V., and Ribbe, P.H. (1971) Quadratic elongation, a quantitative measure of distortion in coordination polyhedra. Science, 172, 567–570.

Rouse, R.C. and Peacor, D.R. (1994) Maricopaite, an unusual lead calcium zeolite with an interrupted mordenite-like framework and intrachannel Pb4 tetrahedral clusters. American Mineralogist, 79, 175-184.

Sheldrick, G. M. (2008) A short history of *SHELX*. Acta Crystallographica, A64, 112-122.

Siidra, O.I., Krivovichev, S.V., and Depmeier, W. (2009) Crystal structure of $Pb_6O[(Si_6Al_2)O_{20}]$. Glass Physics and Chemistry, 35, 406-410.

Smirnov, K.S., Maire, M.L., Brémard, C., and Bougeard, D. (1994) Vibrational spectra of cation-exchanged zeolite A. Experimental and molecular dynamics study. Chemical Physics, 179, 445-454.

Smith, J.V. (1988) Topochemistry of zeolites and related materials. Chemical Reviews, 88, 149-182.

Szymanski, J.T. (1988) The crystal structure of beudadite, $Pb(Fe,Al)_3[(As,S)O_4]_2(OH)_6$.

Canadian Mineralogist, 26, 923-932.

Tribaudino, M., Benna, P., and Bruno, E. (1998) Structural variations induced by thermal treatment in lead feldspar ($PbAl_2Si_2O_8$). American Mineralogist, 83, 159-166.

Wopenka, B., Freeman, J.J., and Nikischer, T. (1998) Raman spectroscopic identification of fibrous natural zeolites. Applied Spectroscopy, 52, 54-63.

Yu, Y., Xiong, G., Li, C., and Xiao, F.-S. (2001) Characterization of aluminosilcate zeolites by UV Raman spectroscopy. Microporous and Mesoporous Materials, 46, 23-34.

List of Tables

Table 1. Powder X-ray diffraction data for rongibbsite.

Table 2. Summary of crystallographic data and refinement results for rongibbsite.

Table 3. Coordinates and displacement parameters of atoms in rongibbsite.

Table 4. Selected non-hydrogen bond distances (Å) in rongibbsite.

Table 5. Bond-valence sums for rongibbsite.

List of Figure Captions

Figure 1. Photograph of rongibbsite crystals.

Figure 2. Crystal structure of rongibbsite. Tetrahedra = TO_4 groups. Large, medium, and small spheres represent Pb, O8H, and H atoms.

Figure 3. A tetrahedral sheet parallel to (101) in rongibbsite.

Figure 4. A variety of tetrahedral rings in the framework structure of rongibbsite.

Figure 5. The complex arrangements of various tetrahedral rings in rongibbsite, viewed (a) along *a* and (b) along *c*. For clarity, the positions of all O, Pb, and H atoms are omitted.

Figure 6. Raman spectrum of rongibbsite.


R100031
500 µm

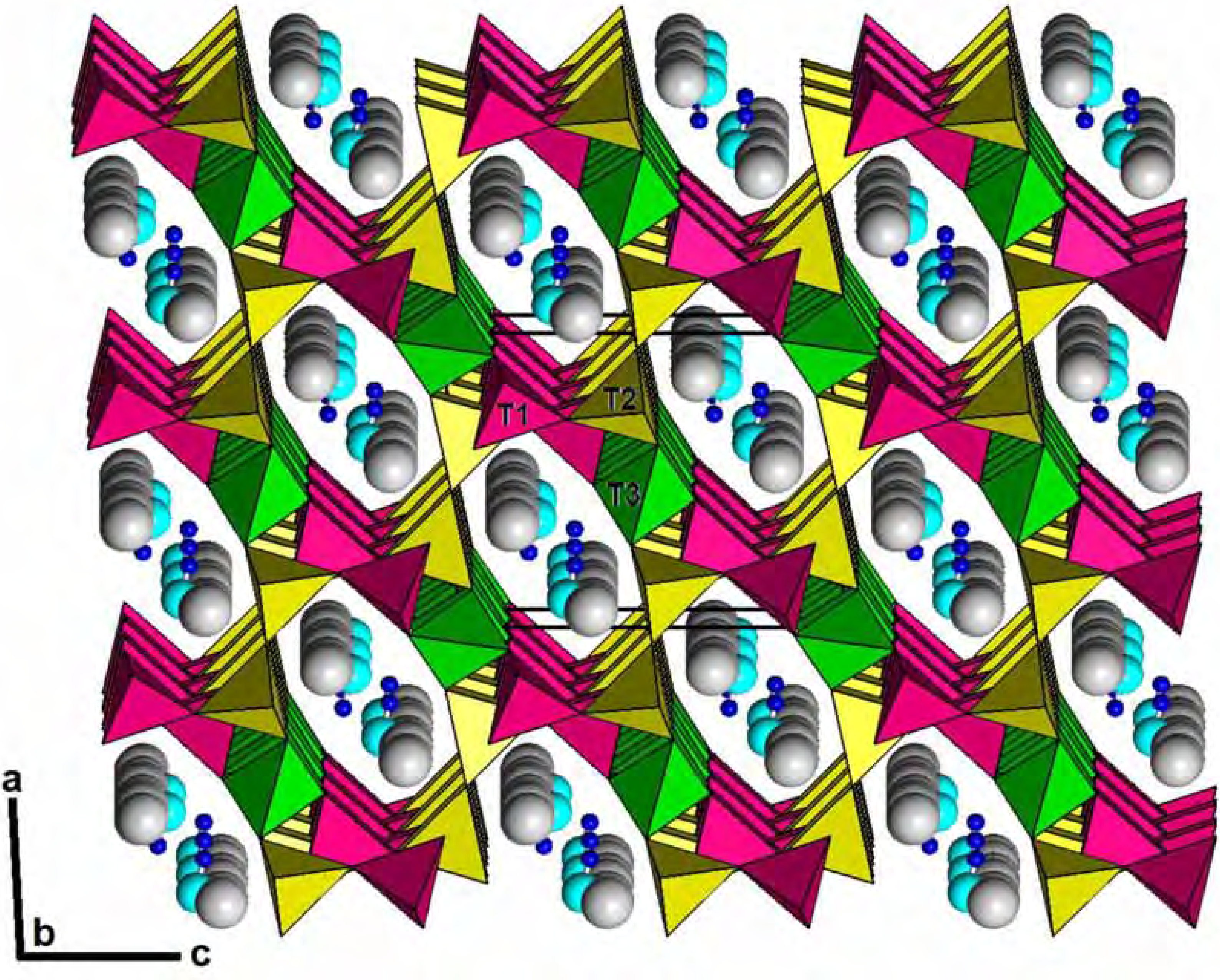

T1
T2
T3
a
b
c

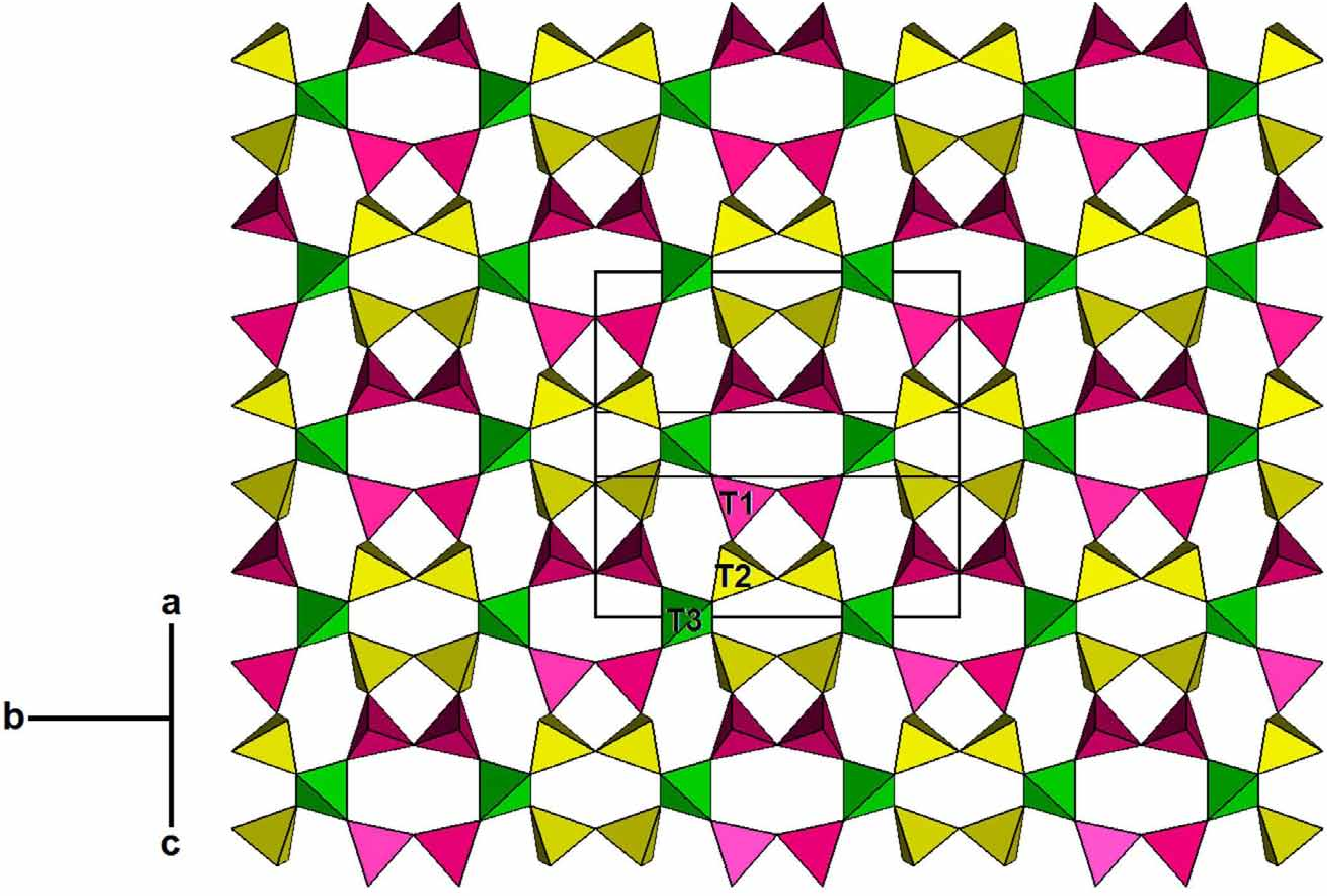
T1
T2
T3
a
b
c

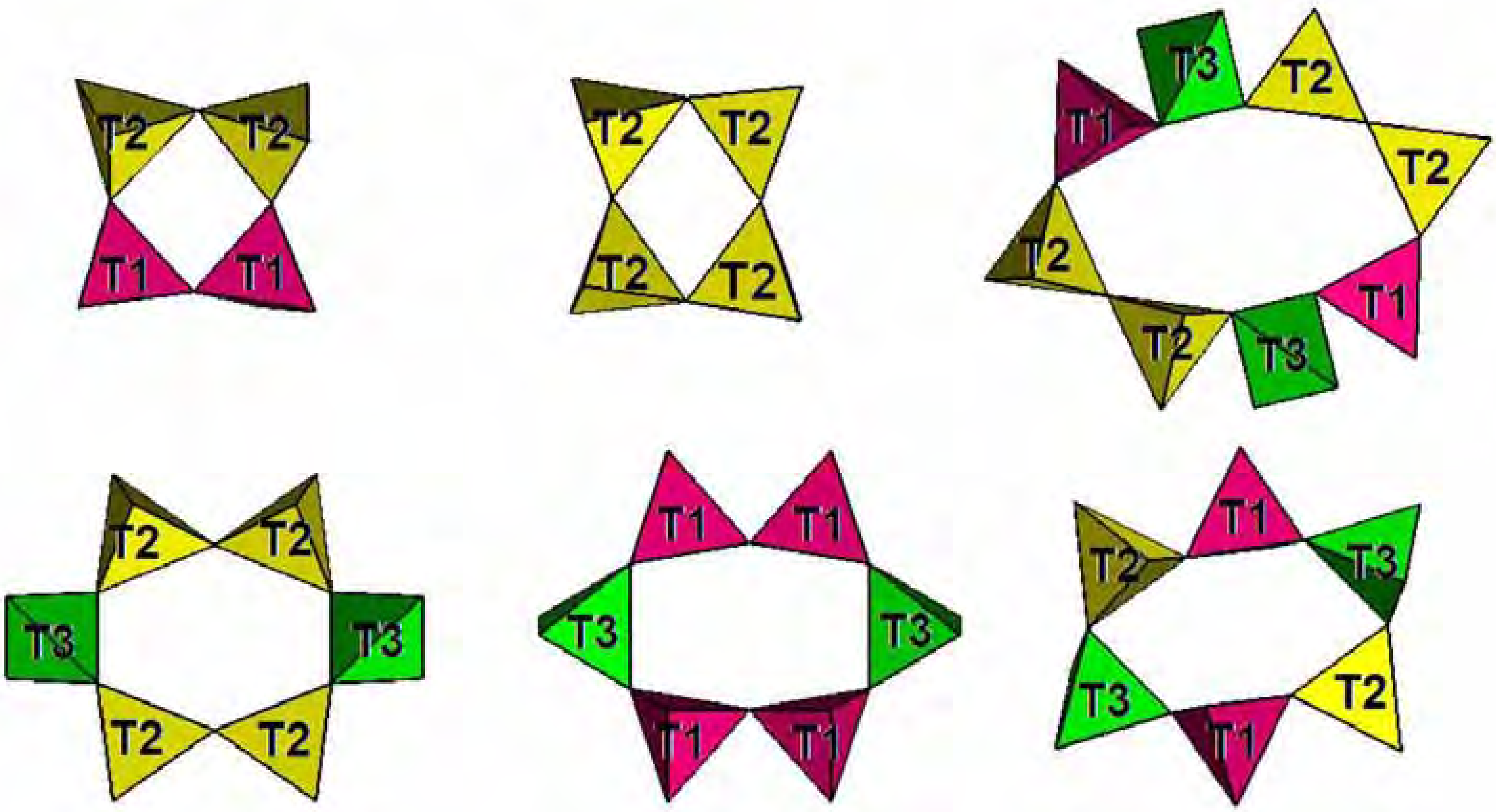
T2
T2
T1
T1
T2
T2
T2
T2
T3
T2
T1
T2
T2
T2
T3
T1
T2
T2
T3
T3
T2
T2
T1
T1
T3
T3
T1
T1
T1
T2
T3
T3
T2
T1

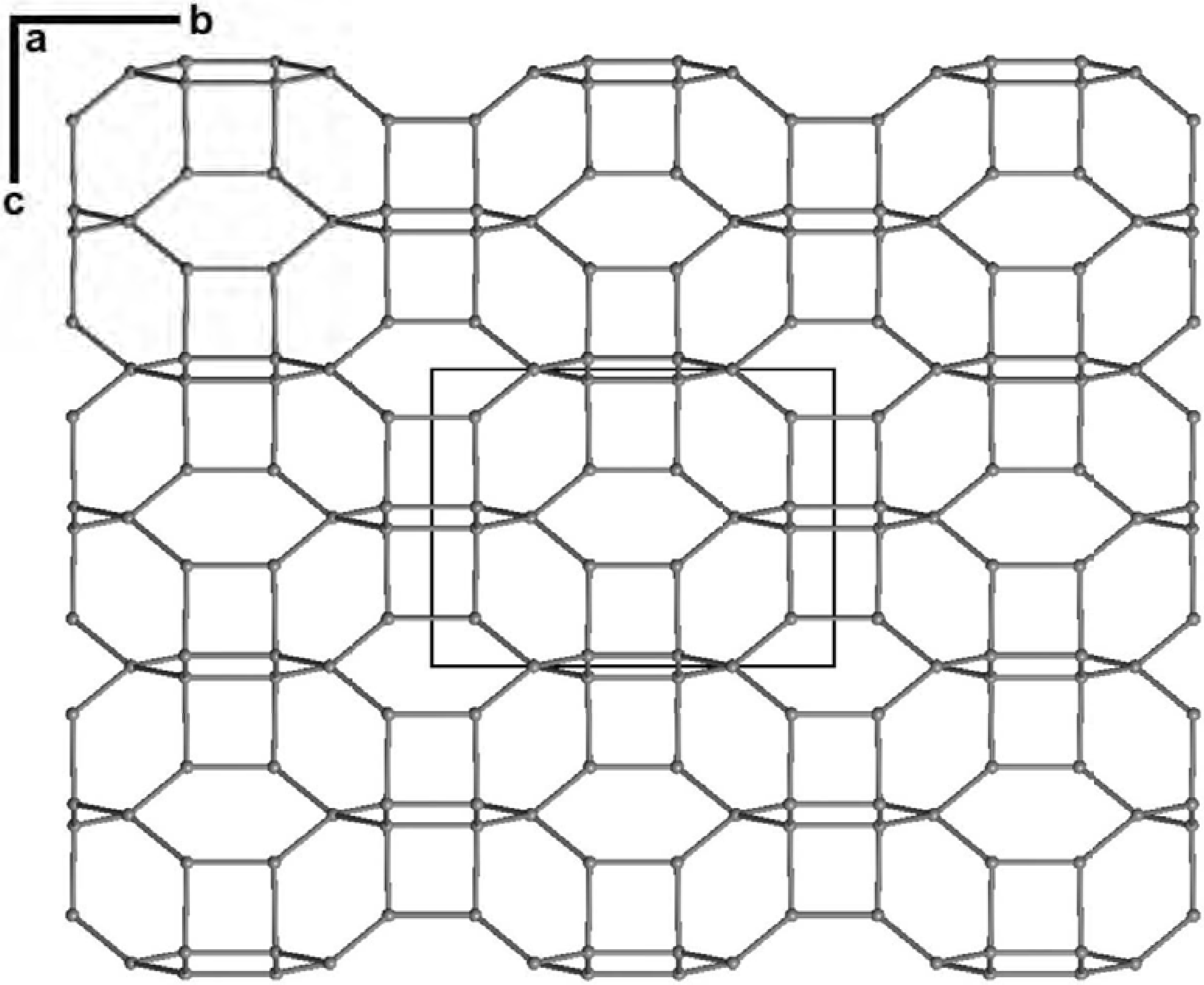
b
a
c

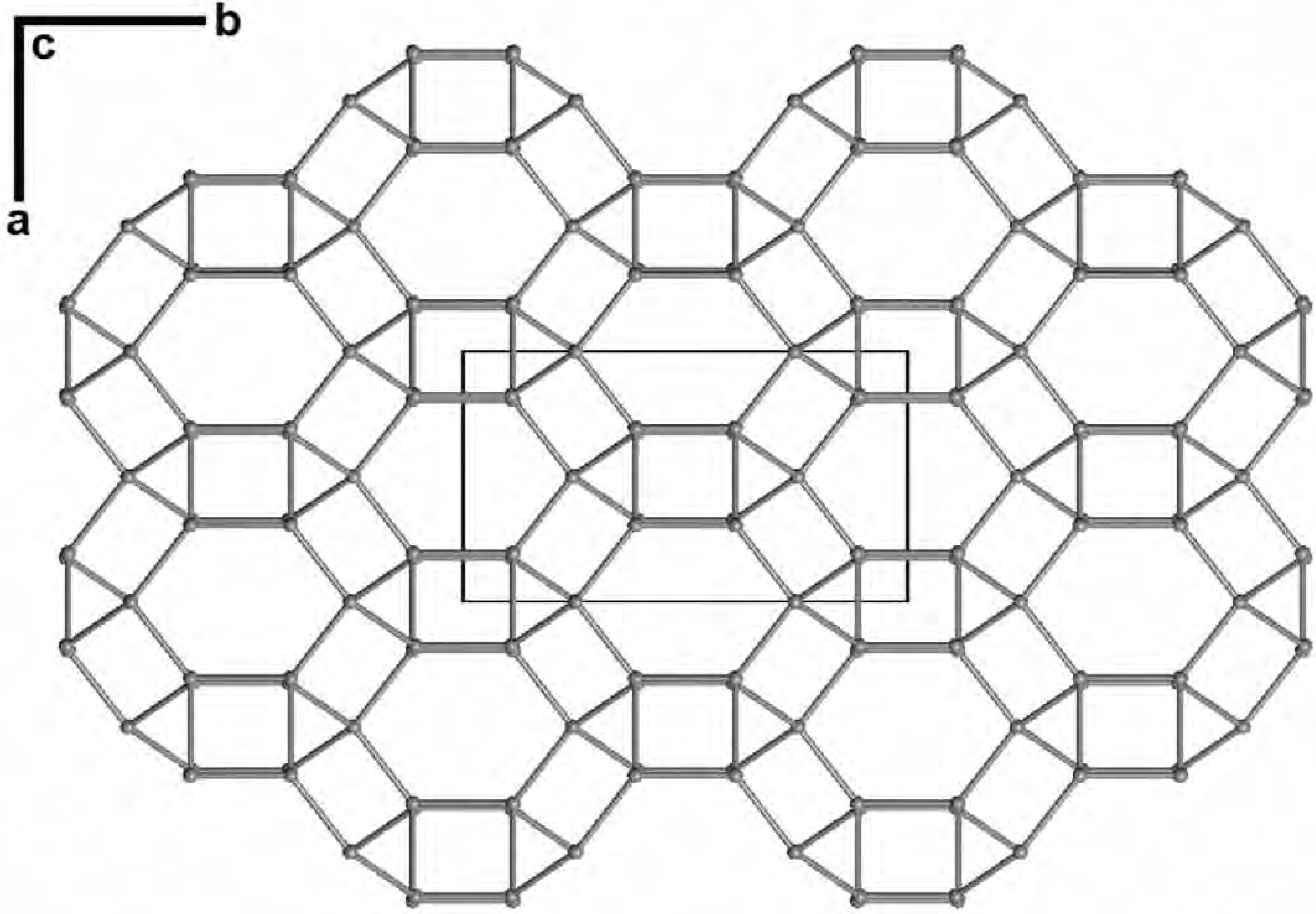
c
b
a

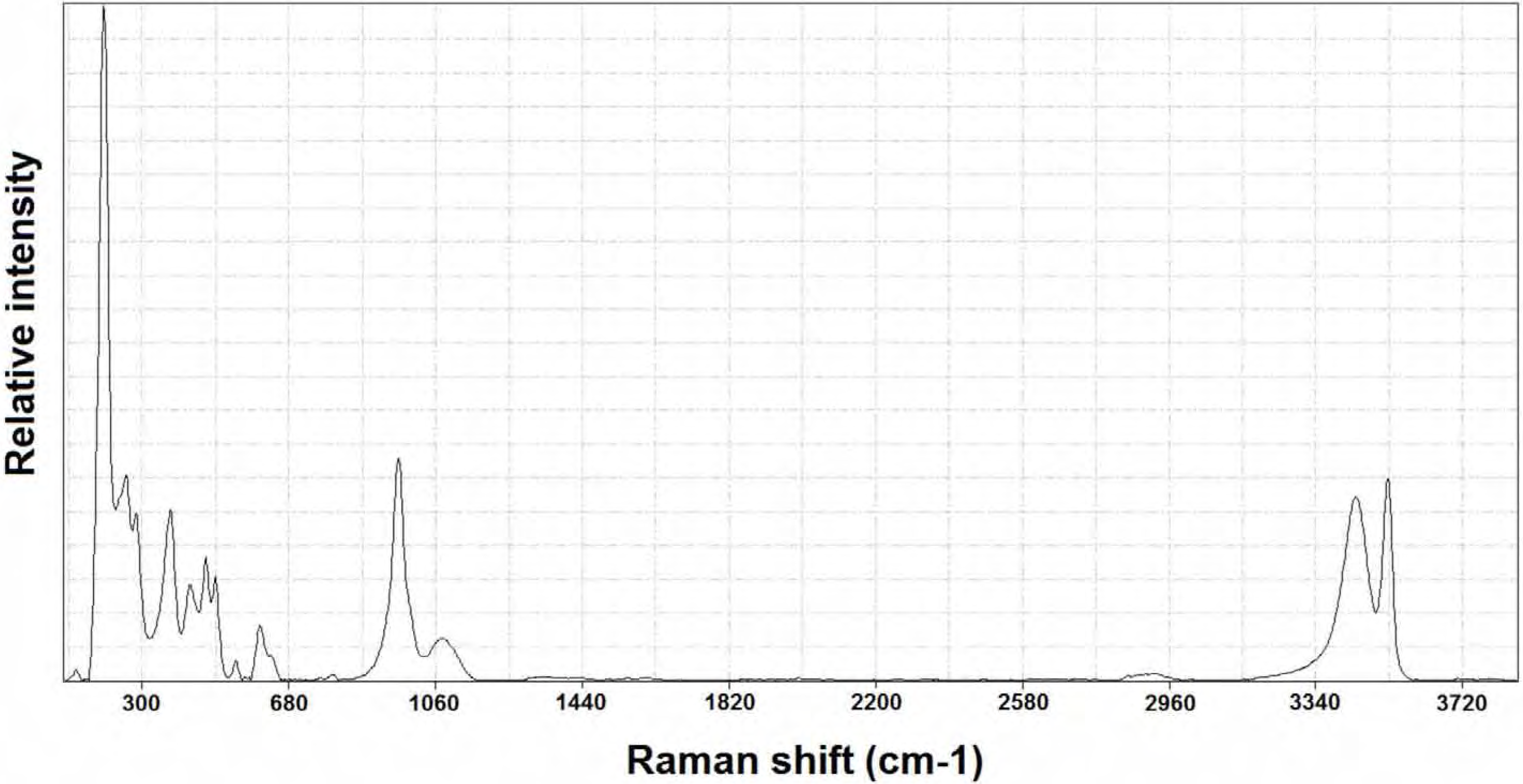
Relative intensity
300
680
1060
1440
1820
2200
2580
2960
3340
3720
Raman shift (cm-1)

Table 1. Powder X-ray diffraction data for rongibbsite based on space group *I*2/*m*.

Intensity	d_{calc}.	h	k	l
68.79	**8.2597**	**0**	**1**	**1**
62.57	**6.9566**	**0**	**2**	**0**
77.48	**6.8206**	**1**	**1**	**0**
8.86	6.3821	-1	0	1
100.00	**6.0754**	**1**	**0**	**1**
5.41	5.1321	0	0	2
4.92	4.7028	-1	2	1
23.89	4.5760	1	2	1
54.18	4.2263	0	3	1
31.19	4.1914	-1	1	2
97.50	**3.9897**	**1**	**3**	**0**
19.71	3.5936	-2	1	1
79.52	**3.4811**	**2**	**1**	**1**
79.78	**3.4783**	**0**	**4**	**0**
7.84	3.4103	2	2	0
74.53	**3.3224**	**0**	**1**	**3**
24.13	3.1953	-1	0	3
59.11	3.1910	-2	0	2
53.82	3.1903	-1	3	2
4.97	3.1109	1	3	2
18.08	3.0777	1	0	3
10.09	3.0542	-1	4	1
26.02	3.0377	2	0	2
22.75	3.0186	1	4	1
16.75	2.9036	-1	2	3
24.24	2.9017	-2	3	1
7.46	2.9004	-2	2	2
3.08	2.8793	0	4	2
89.77	**2.8416**	**2**	**3**	**1**
4.26	2.8146	1	2	3
5.97	2.7839	2	2	2
85.43	**2.7532**	**0**	**3**	**3**
3.56	2.5968	-2	1	3
13.61	2.5660	0	0	4
38.27	2.5595	-3	0	1
9.17	2.4979	3	0	1
3.79	2.4075	0	2	4
5.71	2.4021	-3	2	1
10.14	2.3672	1	1	4
6.89	2.3531	-1	4	3
20.98	2.3514	-2	4	2
6.51	2.3409	-3	1	2
18.95	2.3189	0	6	0
7.38	2.3050	1	4	3
15.06	2.2965	-2	3	3
8.20	2.2880	2	4	2
5.15	2.2735	3	3	0

7.97	2.2489	3	1	2
7.23	2.1978	-2	0	4
29.00	2.1664	1	6	1
29.68	2.1331	1	3	4
21.25	2.1138	-3	3	2
3.32	2.1132	0	6	2
25.14	2.0972	2	0	4
7.90	2.0649	0	4	4
19.09	2.0615	-3	4	1
18.11	2.0453	3	3	2
6.77	2.0289	3	4	1
6.09	2.0110	-1	0	5
3.99	1.9948	2	6	0
6.38	1.9563	4	0	0
4.32	1.9514	0	7	1
9.55	1.9264	1	7	0
6.09	1.9215	-4	1	1
3.22	1.9031	3	5	0
16.26	1.8767	-1	6	3
18.34	1.8759	-2	6	2
4.76	1.8609	-3	1	4
4.10	1.8580	-2	4	4
5.22	1.8520	1	6	3
7.51	1.8432	2	6	2
8.74	1.8409	-2	1	5
9.02	1.8111	-1	7	2
7.96	1.7978	4	0	2
13.30	1.7960	2	4	4
13.69	1.7898	-4	3	1
3.96	1.7664	2	1	5
3.72	1.7530	-2	7	1
5.28	1.7410	-1	4	5
11.99	1.7405	-3	3	4
10.71	1.7395	2	7	1
14.72	1.7241	-2	3	5
7.21	1.7204	0	6	4
9.71	1.7186	0	7	3
8.66	1.7185	-3	6	1
10.22	1.7107	0	0	6
4.31	1.7051	4	4	0
5.44	1.6994	3	6	1

=======================================

Table 2. Summary of crystal data and refinement results for rongibbsite.

Ideal chemical formula	$Pb_2(Si_4Al)O_{11}(OH)$
Crystal symmetry	Monoclinic
Space group	*I*2/*m* (#12)
a(Å)	7.8356(6)
b(Å)	13.913(1)
c(Å)	10.278(1)
α(º)	90
β(º)	92.925(4)
γ(º)	90
V(Å^3)	1119.0(2)
Z	4
ρ_{cal}(g/cm^3)	4.43
λ (Å, Mo *K*α)	0.71073
μ (mm^{-1})	30.62
2θ range for data collection	≤65.14
No. of reflections collected	13044
No. of independent reflections	2107
No. of reflections with $I > 2\sigma(I)$	1750
No. of parameters refined	105
R(int)	0.033
Final R_1, wR_2 factors [$I > 2\sigma(I)$]	0.024, 0.044
Final R_1, wR_2 factors (all data)	0.035, 0.048
Goodness-of-fit	1.067

Table 3. Coordinates and displacement parameters of atoms in rongibbsite

Atom	*x*	*y*	*z*	U_{iso}	U_{11}	U_{22}	U_{33}	U_{23}	U_{13}	U_{12}
Pb	0.0973(2)	0.3460(2)	0.3437(2)	0.0182(2)	0.0230(3)	0.0168(4)	0.0148(2)	-0.0014(2)	-0.0002(3)	0.0033(3)
Pb'	0.1032(9)	0.331(1)	0.3492(8)	0.0277(13)	0.032(1)	0.032(3)	0.018(1)	-0.008(1)	-0.0093(9)	0.019(2)
T1	0.3237(1)	0.3919(1)	0.6610(1)	0.0113(2)	0.0137(5)	0.0101(5)	0.0100(4)	-0.0010(4)	0.0009(4)	0.0002(4)
T2	0.1939(1)	0.1127(1)	0.5361(1)	0.0109(2)	0.0105(5)	0.0101(5)	0.0121(4)	0.0003(4)	0.0000(4)	-0.0002(4)
T3	1/2	0.2465(1)	1/2	0.0073(3)	0.0071(7)	0.0057(6)	0.0092(6)	0	0.0003(5)	0
O1	0.1573(4)	0.3749(2)	0.5630(3)	0.0183(6)	0.018(2)	0.021(1)	0.016(1)	-0.003(1)	-0.002(1)	-0.000(1)
O2	0.3985(5)	1/2	0.6498(4)	0.0167(8)	0.018(2)	0.011(2)	0.022(2)	0	0.006(2)	0
O3	0.4754(4)	0.3177(2)	0.6313(3)	0.0160(6)	0.015(2)	0.013(1)	0.020(1)	-0.004(1)	0.001(1)	0.005(1)
O4	0.2393(4)	0.1248(2)	0.6931(3)	0.0188(6)	0.022(2)	0.020(1)	0.015(1)	0.000(1)	0.004(1)	-0.002(1)
O5	0	0.1551(3)	1/2	0.0214(9)	0.014(2)	0.019(2)	0.031(2)	0	-0.001(2)	0
O6	0.2085(5)	0	0.4893(4)	0.0188(9)	0.025(2)	0.010(2)	0.021(2)	0	0.000(2)	0
O7	0.3299(4)	0.1790(2)	0.4581(3)	0.0174(6)	0.018(2)	0.019(1)	0.016(1)	0.000(1)	0.002(1)	0.001(1)
O8H	0.1282(8)	1/2	0.2839(5)	0.041(1)	0.064(4)	0.025(3)	0.036(3)	0	0.011(3)	0
H	0.24(1)	1/2	0.309(7)	0.03						

Note: Site occupancies are Pb = 0.80, Pb' = 0.20. The Si/Al ratios in the tetrahedral sites are estimated from the bond-valence sums: T1 = Si, T2 = 0.80Si + 0.20Al, T3 = 0.40Si + 0.60Al. The unit for displacement parameters are Å^2.

Table 4. Selected bond distances in rongibbsite

	Distance (Å)		Distance (Å)		Distance (Å)
T1-O1	1.623(3)	T2-O4	1.644(3)	T3-O3	1.693(3) x2
-O2	1.621(2)	-O5	1.654(2)	-O7	1.669(3) x2
-O3	1.615(3)	-O6	1.645(2)		
-O4	1.619(3)	-O7	1.648(3)		
Ave.	1.620		1.648		1.681
Pb-O1	2.292(4)	Pb'-O1	2.300(8)		
-O1	2.315(3)	-O1	2.354(8)		
-O3	3.263(3)	-O3	3.17(1)		
-O3	3.368(3)	-O3	3.231(8)		
-O4	3.160(4)	-O4	3.26(1)		
-O5	3.217(4)	-O5	3.03(2)		
-O7	3.145(4)	-O7	2.94(2)		
-O7	3.201(3)	-O7	3.231(8)		
-O8H	2.245(3)	-O8H	2.46(2)		
Ave.	2.912		2.894		

Table 5. Calculated bond-valence sums for rongibbsite.

	O1	O2	O3	O4	O5	O6	O7	O8H	Sum
Pb	0.615 0.578		0.045 0.033	0.059	0.050x2↓		0.061 0.053	0.698x2↓	1.792
Pb’	0.600 0.520		0.057 0.049	0.045	0.085x2↓		0.106 0.049	0.391x2↓	0.397
T1	1.003	1.008x2↓	1.025	1.014					4.050
T2				0.947	0.922x2↓	0.945x2↓	0.937		3.751
T3			0.830x2→				0.885x2→		3.430
Sum	2.181	2.016	1.938	2.017	1.958	1.890	1.944	1.273	

Note: The bond-valence sum contributions from Pb and Pb’ were scaled by a factor 0.80 and 0.20, respectively, because of the partial occupancies of Pb in these two sites.